JCI The Journal of Clinical Investigation

Genetically engineered *SCN5A* mutant pig hearts exhibit conduction defects and arrhythmias

David S. Park, Marina Cerrone, Gregory Morley, Carolina Vasquez, Steven Fowler, Nian Liu, Scott A. Bernstein, Fang-Yu Liu, Jie Zhang, Christopher S. Rogers, Silvia G. Priori, Larry A. Chinitz, Glenn I. Fishman

J Clin Invest. 2015;125(1):403-412. https://doi.org/10.1172/JCI76919.

Research Article

SCN5A encodes the α subunit of the major cardiac sodium channel $Na_V1.5$. Mutations in *SCN5A* are associated with conduction disease and ventricular fibrillation (VF); however, the mechanisms that link loss of sodium channel function to arrhythmic instability remain unresolved. Here, we generated a large-animal model of a human cardiac sodium channelopathy in pigs, which have cardiac structure and function similar to humans, to better define the arrhythmic substrate. We introduced a nonsense mutation originally identified in a child with Brugada syndrome into the orthologous position (E558X) in the pig *SCN5A* gene. $SCN5A^{E558X/+}$ pigs exhibited conduction abnormalities in the absence of cardiac structural defects. Sudden cardiac death was not observed in young pigs; however, Langendorff-perfused $SCN5A^{E558X/+}$ hearts had an increased propensity for pacing-induced or spontaneous VF initiated by short-coupled ventricular premature beats. Optical mapping during VF showed that activity often began as an organized focal source or broad wavefront on the right ventricular (RV) free wall. Together, the results from this study demonstrate that the $SCN5A^{E558X/+}$ pig model accurately phenocopies many aspects of human cardiac sodium channelopathy, including conduction slowing and increased susceptibility to ventricular arrhythmias.

Genetically engineered *SCN5A* mutant pig hearts exhibit conduction defects and arrhythmias

David S. Park,[1,2] Marina Cerrone,[1] Gregory Morley,[1] Carolina Vasquez,[1] Steven Fowler,[1,2] Nian Liu,[1] Scott A. Bernstein,[1,2] Fang-Yu Liu,[1] Jie Zhang,[1] Christopher S. Rogers,[3] Silvia G. Priori,[1,4] Larry A. Chinitz,[1,2] and Glenn I. Fishman[1]

[1]Leon H. Charney Division of Cardiology and [2]Heart Rhythm Center, New York University School of Medicine, New York, New York, USA. [3]Exemplar Genetics, Coralville, Iowa, USA. [4]Fondazione Maugeri IRCCS, Department of Molecular Medicine, University of Pavia, Pavia, Italy.

SCN5A **encodes the α subunit of the major cardiac sodium channel $Na_V1.5$. Mutations in *SCN5A* are associated with conduction disease and ventricular fibrillation (VF); however, the mechanisms that link loss of sodium channel function to arrhythmic instability remain unresolved. Here, we generated a large-animal model of a human cardiac sodium channelopathy in pigs, which have cardiac structure and function similar to humans, to better define the arrhythmic substrate. We introduced a nonsense mutation originally identified in a child with Brugada syndrome into the orthologous position (E558X) in the pig *SCN5A* gene. *$SCN5A^{E558X/+}$* pigs exhibited conduction abnormalities in the absence of cardiac structural defects. Sudden cardiac death was not observed in young pigs; however, Langendorff-perfused *$SCN5A^{E558X/+}$* hearts had an increased propensity for pacing-induced or spontaneous VF initiated by short-coupled ventricular premature beats. Optical mapping during VF showed that activity often began as an organized focal source or broad wavefront on the right ventricular (RV) free wall. Together, the results from this study demonstrate that the *$SCN5A^{E558X/+}$* pig model accurately phenocopies many aspects of human cardiac sodium channelopathy, including conduction slowing and increased susceptibility to ventricular arrhythmias.**

Introduction

The pore-forming subunit of the cardiac sodium channel ($Na_V1.5$; encoded by *SCN5A*) is a critical determinant of myocardial excitability and conduction. Loss-of-function mutations in *SCN5A* diminish the magnitude of the inward sodium current (I_{Na}) and can clinically manifest as progressive cardiac conduction disorders (PCCD) (1, 2) or as arrhythmic syndromes, which include Brugada syndrome (BrS) (3) and atrial fibrillation (4). In addition to electrophysiological dysfunction, *SCN5A* mutations are also associated with myocardial fibrosis that can be regionally localized or diffuse, manifesting as a global cardiomyopathy (5). This broad phenotypic expressivity of *SCN5A* mutations has made it difficult to draw direct connections between sodium channel dysfunction and arrhythmic susceptibility.

The prototypical loss-of-function *SCN5A* condition, BrS, is one such example in which the mechanism linking reduced I_{Na} to ventricular arrhythmias is uncertain. BrS is associated with sudden death due to polymorphic ventricular tachycardia (PMVT) and ventricular fibrillation (VF) and is diagnosed by the ECG pattern of coved-type ST elevation with terminal T-wave inversions in leads V1–V3, which can be stable or transient (6). Mutations in *SCN5A* have been identified in 20%–30% of BrS patients, and mutant carriers typically manifest some level of conduction disease (1, 7, 8). However, not all loss-of-function *SCN5A* mutations associated with ventricular tachycardia or VF exhibit BrS-pattern ECG (9, 10). These findings highlight the complex relationship between *SCN5A* mutations and ventricular arrhythmias and underscore the need to better define the arrhythmic substrate in cardiac sodium channelopathies. To that end, we took advantage of emerging technologies (11) to create genetically engineered pigs harboring a nonsense mutation in *SCN5A*. The pig offers several advantages for the study of human arrhythmic conditions due to similarities in heart rate, cardiac size, anatomy, action potential shape, and autonomic innervation (12). Thus, the pig model is a compelling platform to investigate arrhythmia mechanisms and to test new therapeutic modalities. Here we report the development and characterization of the first porcine model of a human cardiac sodium channelopathy. We found that pigs with the mutation E555X introduced into the orthologous position in the *SCN5A* gene (referred to herein as *$SCN5A^{E558X/+}$*) had reduced expression of $Na_V1.5$ protein, which resulted in diminished total sodium conductance. *$SCN5A^{E558X/+}$* hearts demonstrated slowed conduction in the absence of structural defects of the myocardium or specialized conduction system. Although sudden cardiac death was not observed during the first 2 years of life, *$SCN5A^{E558X/+}$* hearts were highly arrhythmic when Langendorff perfused, displaying spontaneous and inducible VF.

▶ Related Article: p. 99

Conflict of interest: Christopher S. Rogers is an employee and shareholder of Exemplar Genetics.
Submitted: May 7, 2014; **Accepted:** October 16, 2014.
Reference information: *J Clin Invest*. 2015;125(1):403–412. doi:10.1172/JCI76919.

Results

Generation of a porcine model of a cardiac sodium channelopathy. We selected a single amino acid substitution leading to a premature stop codon mutation causing early protein truncation at amino acid 558 (E558X). The orthologous human mutation (E555X) was initially detected in a 10-year-old child who presented with fever,

atrial flutter, nonsustained PMVT, and coved-type ST elevations on ECG. Baseline ECG of the child demonstrated sinus rhythm alternating with sinus bradycardia, normal QRS axis, upper limits of normal PR interval for age (170 ms), prolonged QRS duration (120 ms), and normal corrected QT interval (419 ms) (Supplemental Figure 1; supplemental material available online with this article; doi:10.1172/JCI76919DS1). Flecainide infusion reproduced coved-type ST elevations in leads V1–V2 (Figure 1A), confirming the diagnosis of BrS. This mutation was selected based on the potential for earlier clinical manifestation of sodium channelopathy coupled with the severity of the premature truncation mutation.

Cardiac sodium channelopathy pigs were generated by homologous recombination in fibroblasts from outbred domestic Yucatan mini pigs (11). The E558X premature stop mutation was introduced into the porcine *SCN5A* gene, followed by somatic cell nuclear transfer to generate *SCN5A*$^{E558X/+}$ heterozygous offspring (Figure 1, B–E). *SCN5A*$^{E558X/+}$ animals were viable and fertile. Over a 2-year monitoring period, sudden death was not observed in WT or *SCN5A*$^{E558X/+}$ pigs.

Diminished $Na_V1.5$ protein levels and I_{Na} density in SCN5A$^{E558X/+}$ cardiomyocytes. Expression of $Na_V1.5$ was examined by Western blot (WB) analysis on isolated membrane preparations (Figure 1F). The relative expression of $Na_V1.5$ was significantly reduced in *SCN5A*$^{E558X/+}$ right and left ventricular outflow tracts (RVOT and LVOT, respectively) compared with WT littermate controls (RVOT, 0.55 ± 0.033, $P < 0.002$; LVOT, 0.75 ± 0.015, $P < 0.02$; Figure 1G). There was no significant difference in the level of $Na_V1.5$ between *SCN5A*$^{E558X/+}$ RVOT and LVOT (data not shown). Immunolocalization of $Na_V1.5$ with N-cadherin (N-cad) at the intercalated discs was unperturbed in *SCN5A*$^{E558X/+}$ cardiomyocytes (Supplemental Figure 2). Decreased $Na_V1.5$ protein expression was associated with diminished I_{Na} density in *SCN5A*$^{E558X/+}$ atrial myocytes (Figure 1H). Average I_{Na} density–voltage plots showed a significant reduction in I_{Na} density at several tested voltages compared with WT atrial myocytes (–50 mV, WT, 66.78 ± 6.16 pA/pF; *SCN5A*$^{E558X/+}$, 23.44 ± 4.96 pA/pF; $P = 3.32 \times 10^{-4}$; Figure 1H).

In vivo electrophysiological analysis of SCN5A$^{E558X/+}$ animals demonstrates slow conduction. Baseline ECGs were obtained from WT (n = 18, age 17 ± 5 months) and *SCN5A*$^{E558X/+}$ (n = 19, age 16 ± 5 months) pigs sedated with inhaled isoflurane. Figure 2, A and B, shows representative lead II traces and average ECG intervals. *SCN5A*$^{E558X/+}$ animals had prolonged P and QRS wave duration and prolonged PR intervals, consistent with slowed conduction. Comprehensive electrophysiology study (EPS) was performed on WT (n = 8, age 21 ± 2 months) and *SCN5A*$^{E558X/+}$ (n = 8, age 21 ± 2 months) anesthetized animals. Baseline intracardiac measurements demonstrated prolonged atrial-His and His-ventricular conduction intervals in *SCN5A*$^{E558X/+}$ pigs (Figure 2C), consistent with conduction slowing through the atrioventricular (AV) node and His-Purkinje system (HPS), respectively. Functional assessments of the sinoatrial and AV nodes demonstrated significantly prolonged corrected sinus node recovery time and AV Wenckebach cycle length, respectively, in *SCN5A*$^{E558X/+}$ animals (Figure 2D). Therefore, *SCN5A*$^{E558X/+}$ pigs accurately phenocopy conduction disease, including abnormalities of the specialized conduction system, seen in patients with loss-of-function sodium channel mutations (1, 8, 13, 14).

Response to flecainide challenge in SCN5A$^{E558X/+}$ pigs. Sodium channel blocker challenge with flecainide, ajmaline, or procainamide is known to accentuate ECG features, such as conduction and repolarization abnormalities, in patients with *SCN5A* mutations (6, 15). In patients with BrS, sodium channel blockers can produce diagnostic ECG changes characterized by coved-type ST elevations with terminal T-wave inversions in the precordial leads (6, 15). Accordingly, we examined the effects of graded infusions of flecainide in 2 groups of animals: a young cohort of WT (n = 6, age 4 ± 1 months) and *SCN5A*$^{E558X/+}$ (n = 5, age 4 months) pigs and an adult cohort of WT (n = 5, age 10 ± 1 months) and *SCN5A*$^{E558X/+}$ (n = 5, age 15 ± 2 months) pigs. Conduction disease was present in *SCN5A*$^{E558X/+}$ pigs of both young and adult cohorts at baseline and in response to low-dose flecainide (1 mg/kg) (Figure 2E). Furthermore, adult *SCN5A*$^{E558X/+}$ animals showed a significant increase in PR and QRS durations with flecainide compared with *SCN5A*$^{E558X/+}$ pigs of the young cohort, whereas WT animals did not show the same age-dependent response to sodium channel blockade (Figure 2F). Representative lead II ECG traces from adult WT and *SCN5A*$^{E558X/+}$ animals before and after flecainide treatment are shown in Figure 2G. Moreover, a subset of *SCN5A*$^{E558X/+}$ pigs in both age groups developed second-degree AV block in response to sodium channel blocker challenge (young cohort, 3 of 5; adult cohort, 4 of 5; Figure 2H). In contrast, WT animals exhibited only modest ECG changes with full-dose flecainide (2 mg/kg) (data not shown). Despite enhanced sensitivity to sodium channel blockers, BrS-type ECG changes were not observed in *SCN5A*$^{E558X/+}$ animals.

Absence of structural remodeling in SCN5A$^{E558X/+}$ hearts. To evaluate whether the conduction abnormalities observed in *SCN5A*$^{E558X/+}$ hearts are associated with localized or diffuse fibrotic changes, WT and *SCN5A*$^{E558X/+}$ hearts were subjected to transthoracic echocardiography (TTE), electroanatomic mapping, and histological evaluation. In vivo structural and functional assessments were obtained from adult WT (n = 5, age 21 ± 1 months) and *SCN5A*$^{E558X/+}$ (n = 7, age 22 ± 1 months) animals using TTE. Left and right ventricular (LV and RV, respectively) size and function were not significantly different in *SCN5A*$^{E558X/+}$ versus WT hearts (Supplemental Table 1). To evaluate for subclinical fibrosis in *SCN5A*$^{E558X/+}$ ventricles, we performed endocardial and epicardial voltage mapping using the EnSite Velocity Cardiac Mapping System (St. Jude Medical Inc.) and histological analysis (n = 3 each, WT and *SCN5A*$^{E558X/+}$, age 20 ± 1 months). There was no evidence of low-voltage (<1.5 mV) bipolar electrogram signals in the RV endocardium or epicardium of *SCN5A*$^{E558X/+}$ hearts (Supplemental Figure 3). However, average bipolar electrogram durations (n = 10 recordings from each region) measured from the RVOT endocardium and epicardium were significantly longer in *SCN5A*$^{E558X/+}$ hearts (RVOT endocardium, WT, 59.6 ± 5 ms; *SCN5A*$^{E558X/+}$, 67.1 ± 6.9 ms, $P < 0.00002$; RVOT epicardium, WT, 57.9 ± 3.5 ms; *SCN5A*$^{E558X/+}$, 65.4 ± 5 ms, $P < 8 \times 10^{-9}$; Supplemental Figure 4). Detailed inspection of the specialized conduction system and outflow tract regions using Masson's trichrome stain did not reveal increased fibrosis in *SCN5A*$^{E558X/+}$ hearts (WT, n = 5, age 8 ± 1 months; *SCN5A*$^{E558X/+}$, n = 5, age 7 months; Figure 3). H&E and Masson's trichrome staining performed on outflow tract regions of older WT and *SCN5A*$^{E558X/+}$ animals (n = 3 each, age 20 ± 1 months) did not

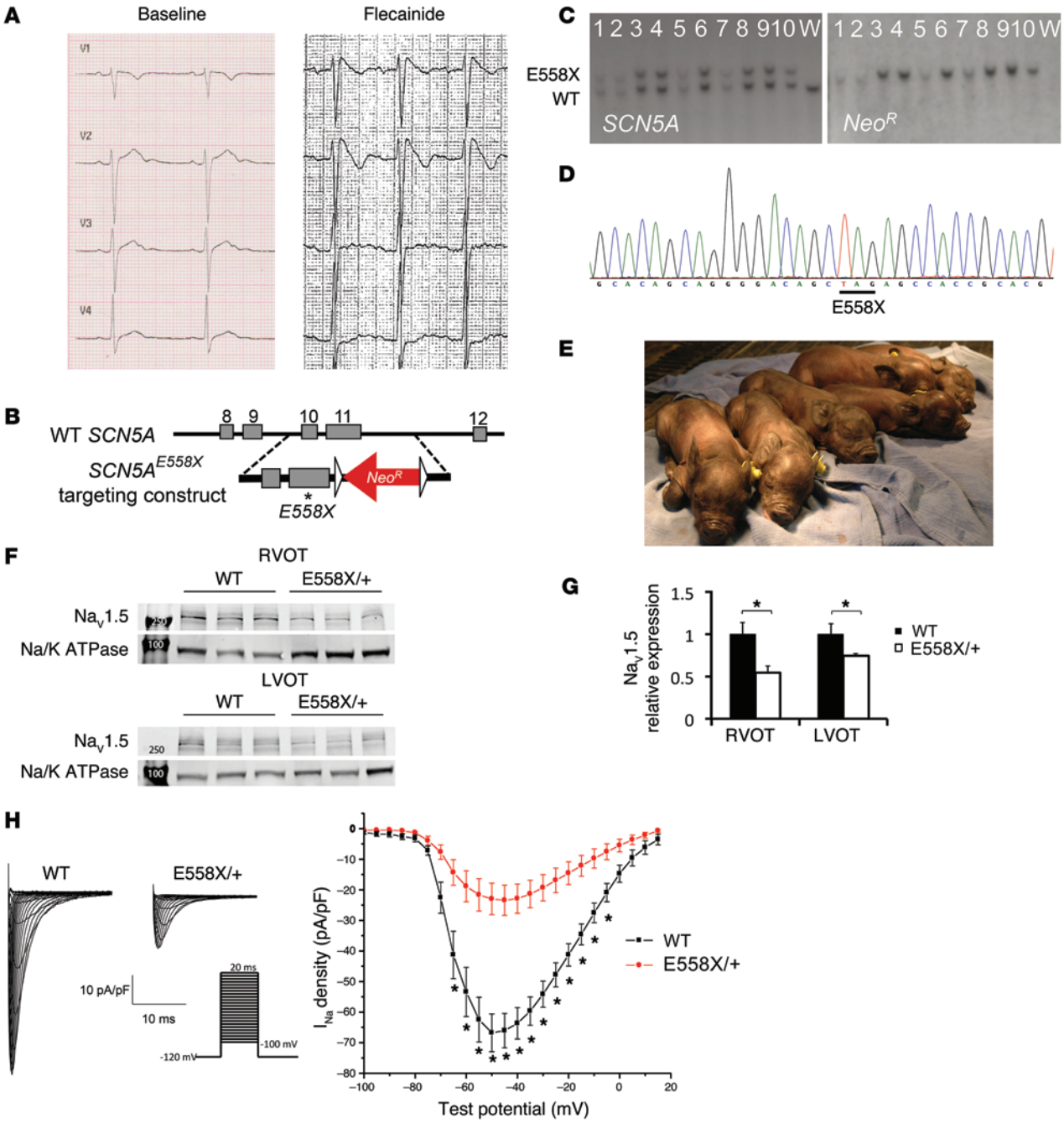

Figure 1. Generation of *SCN5A*$^{E558X/+}$ pigs. (**A**) Precordial lead ECG from the 10-year-old child with *SCN5A*$^{E555X/+}$ mutation, at baseline and during flecainide challenge. (**B**) The targeting vector contains a G-to-T point mutation (asterisk), resulting in replacement of a glutamic acid at amino acid 558 with a premature stop codon (GAG to TAG), as well as a floxed (triangles) neomycin resistance cassette (Neo^R) driven by the phosphoglycerate kinase promoter in intron 11 for selection. (**C** and **D**) Properly targeted cells were identified by Southern blot (**C**) and direct sequencing (**D**). (**E**) Yucatan mini pigs harboring a single copy of the *SCN5A*^{E558X} mutation (*SCN5A*$^{E558X/+}$ pigs; E558X/+) were viable and appeared grossly normal. (**F**) WBs of membrane fractions detecting $Na_V1.5$ and the sodium-potassium ATPase (Na/K ATPase) as loading control. Molecular weight markers (250 and 100 kDa) are indicated in lane 1. (**G**) $Na_V1.5$ protein levels (normalized to Na/K ATPase), displayed relative to WT. *$P < 0.05$. (**H**) Patch-clamp analysis of atrial myocytes. Shown are representative whole-cell Na^+ current recordings and average current/voltage relationship from adult WT ($n = 23$ cells) and *SCN5A*$^{E558X/+}$ ($n = 16$ cells) left atrial myocytes. *$P < 0.01$.

show evidence of myocyte hypertrophy, disarray, or fibrosis in *SCN5A*$^{E558X/+}$ hearts (data not shown). Although animals older than 2 years could conceivably develop fibrosis, the histology of the adult mutant pigs studied to date is consistent with an isolated channelopathy phenotype, without macroscopic or microscopic structural alterations.

SCN5A$^{E558X/+}$ *ventricular myocytes do not show significant remodeling at the protein level.* $Na_V1.5$ preferentially localizes at intercalated discs through interactions with the voltage-gated sodium channel (VGSC) complex (16). The VGSC complex allows physical and functional interactions between desmosomal, gap junction, and adherens junction components (17). Consequently, loss of the

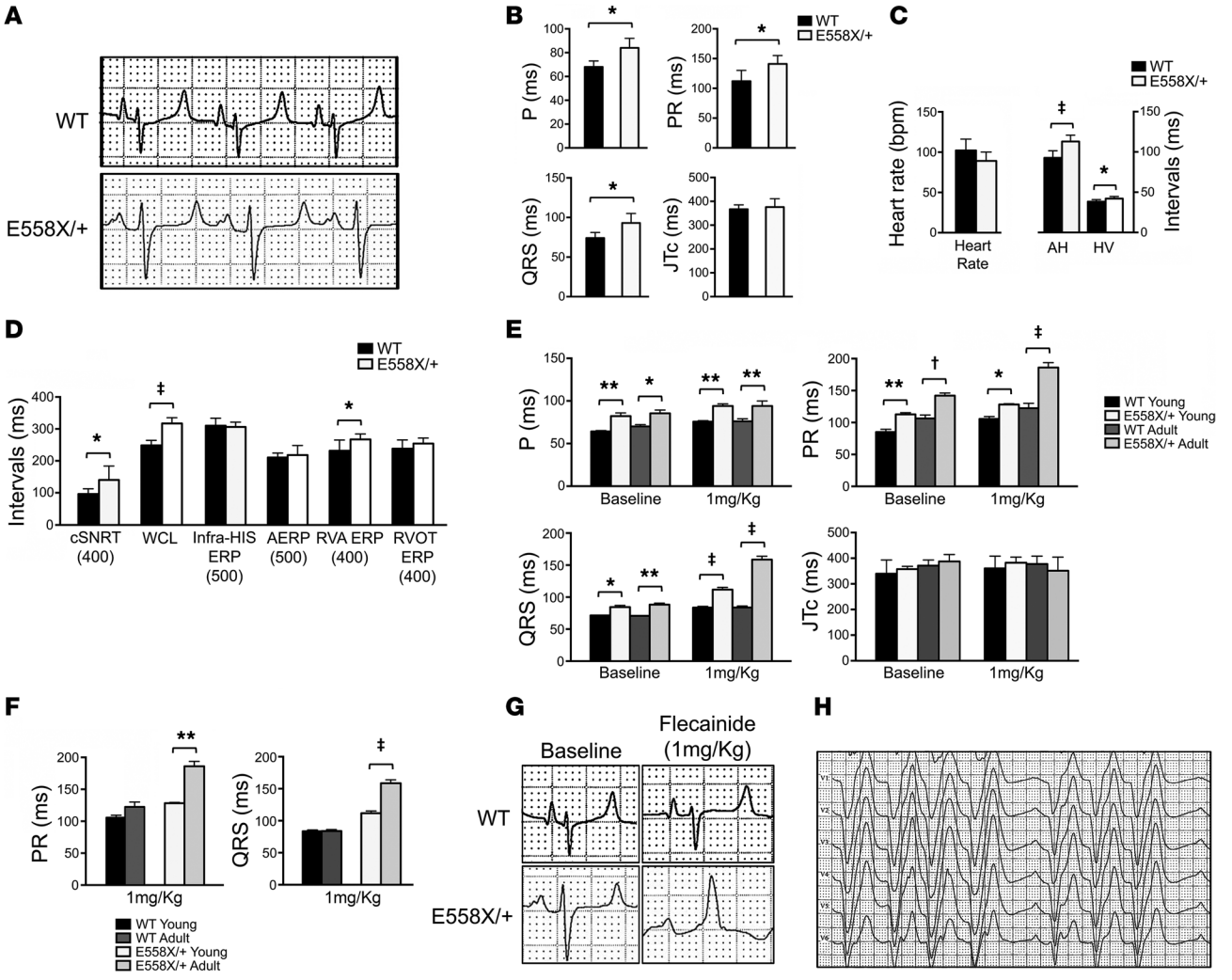

Figure 2. Electrophysiological analysis of *SCN5A*$^{E558X/+}$ pigs at baseline and during sodium channel blocker challenge. (**A**) Representative ECG traces (lead II) of WT and *SCN5A*$^{E558X/+}$ pigs. (**B**) Average P and QRS wave duration, as well as average PR and JTc intervals at baseline, in WT (n = 18, age 17 ± 5 months) and *SCN5A*$^{E558X/+}$ (n = 19, age 16 ± 5 months) pigs. *P < 0.001. (**C** and **D**) Comprehensive EPS was performed on WT (n = 8, age 22 ± 2 months) and *SCN5A*$^{E558X/+}$ (n = 8, age 22 ± 1 months) pigs. (**C**) Average baseline intracardiac intervals. AH, atrial-His; HV, His-ventricular. (**D**) Average electrophysiological parameters. Basic cycle length (in ms) is shown below. cSNRT, corrected sinus node recovery time; WCL, Wenckebach cycle length, ERP, effective refractory period; AERP, atrial ERP. *P < 0.05; ‡P < 0.00001. (**E** and **F**) Flecainide challenge was performed in 2 groups of animals: a young cohort of WT (n = 6, age 4 ± 1 months) and *SCN5A*$^{E558X/+}$ (n = 5, age 4 months) pigs, and an adult cohort of WT (n = 5, age 10 ± 1 months) and *SCN5A*$^{E558X/+}$ (n = 5, age 15 ± 2 months) pigs. (**E**) Average P, PR, QRS, and JTc intervals at baseline and after 1 mg/kg flecainide challenge. *P < 0.05; **P < 0.01; †P < 0.001; ‡P < 0.0001. (**F**) Average PR and QRS increase after 1 mg/kg flecainide challenge. **P < 0.02; ‡P < 0.0001. (**G**) Representative ECG traces (lead II) in adult WT and *SCN5A*$^{E558X/+}$ pigs at baseline and after infusion of 1 mg/kg flecainide. (**H**) Representative precordial lead ECG of an adult *SCN5A*$^{E558X/+}$ pig after administration of 1 mg/kg flecainide.

gap junction protein connexin 43 (Cx43), or the desmosomal protein plakophilin 2 (PKP2), results in diminished $Na_v1.5$ expression at intercalated discs (18, 19). Furthermore, it has recently been shown that $Na_v1.5$ and Kir2.1 exist in a macromolecular complex with synapse-associated protein 97 (SAP97) (20). Based on these known interactions, we examined *SCN5A*$^{E558X/+}$ hearts for changes in protein expression and localization at the intercalated discs of key protein constituents of the VGSC complex. Despite the reduction in $Na_v1.5$, expression in SAP97, ankyrin G (AnkG), N-cad, and Cx43 were unchanged (Supplemental Figure 5). To evaluate whether reduced $Na_v1.5$ expression results in altered localization of VGSC complex proteins, immunostaining was performed on freshly prepared RVOT and LVOT sections. Immunolocalization patterns of desmoplakin, AnkG, Cx43, N-cad, zonula occludens 1 (ZO-1), and SAP97 in *SCN5A*$^{E558X/+}$ hearts were similar to those of controls (Supplemental Figure 6). These data suggest that heterozygous expression of $Na_v1.5$ is sufficient to maintain the VGSC complex at intercalated discs at this age.

SCN5A$^{E558X/+}$ *hearts display reduced conduction velocity (CV).* Regional heterogeneities in depolarization and repolarization have been proposed as the arrhythmic substrate in loss-of-function *SCN5A* mutant hearts (21). To evaluate for depolarization and repolarization heterogeneities, WT (n = 4, age 22 ± 1 months) and *SCN5A*$^{E558X/+}$ (n = 4, age 22 ± 1 months) hearts were excised, Langendorff perfused, and subjected to high-resolution optical mapping. Figure 4, A–C, shows representative examples of brightfield

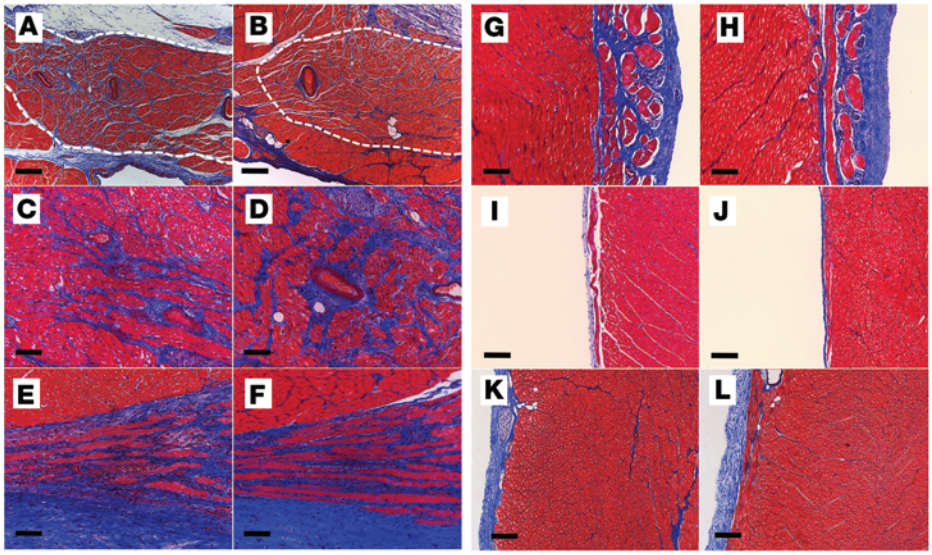

Figure 3. Cardiac structural evaluation of *SCN5A*$^{E558X/+}$ pigs. WT (**A**, **C**, **E**, **G**, **I**, and **K**) and *SCN5A*$^{E558X/+}$ (**B**, **D**, **F**, **H**, **J**, and **L**) hearts were evaluated for fibrosis using Masson's trichrome stain. Shown are representative sections from the sinoatrial node (**A** and **B**; dashed white outlines), AV node (**C** and **D**), proximal His bundle (**E** and **F**), left bundle branch (**G** and **H**), right bundle branch (**I** and **J**), and RVOT (**K** and **L**). Scale bars: 100 μm (**A**–**J**); 200 μm (**K** and **L**).

images of the preparation and activation maps of the RV free wall from WT and *SCN5A*$^{E558X/+}$ hearts obtained at the indicated pacing cycle lengths. Epicardial CVs were substantially reduced in *SCN5A*$^{E558X/+}$ versus WT hearts, as evidenced by reduced spacing of isochronal lines in the *SCN5A*$^{E558X/+}$ activation maps. Average CVs were separately measured in the RV apex (RVA) and RVOT, which demonstrated similar reductions in these myocardial regions in *SCN5A*$^{E558X/+}$ hearts (Figure 4D). Action potential durations (APDs) measured from the RVA and RVOT were not significantly different between the WT and *SCN5A*$^{E558X/+}$ groups (Figure 4E).

SCN5A$^{E558X/+}$ *hearts have increased susceptibility to VF*. Initial attempts at optical mapping of *SCN5A*$^{E558X/+}$ hearts at a normothermic perfusion temperature of 39°C (protocol 1) resulted in spontaneous, intractable VF in 3 of 3 *SCN5A*$^{E558X/+}$ hearts (age 20 ± 1 months), whereas 2 WT hearts (age 19 months) were rhythmically stable under the same conditions (Figure 5A). Spontaneous VF episodes in *SCN5A*$^{E558X/+}$ hearts were initiated by single or repetitive short-coupled premature ventricular beats (VPBs) with an average coupling interval of 316 ± 55 ms (Figure 5B). WT hearts challenged with high-dose flecainide (up to 3 μM) did not induce spontaneous VF despite significant QRS prolongation (Supplemental Figure 7). In an attempt to diminish the spontaneous fibrillatory activity, the protocol was modified to a starting perfusion temperature at 35°C with a slow ramp to 37°C (protocol 2). *SCN5A*$^{E558X/+}$ hearts, while stable at 35°C, during the ramp to 37°C, still underwent spontaneous episodes of VF in 2 of 5 animals (n = 5, age 22 ± 1 months), and during perfusion at a steady-state temperature of 37°C, 4 of 5 hearts had inducible VF, which was triggered during the pacing protocol used to obtain CV and APD measurements. In contrast, no spontaneous or inducible arrhythmias were evident in WT hearts (n = 5, age 21 ± 1 months) during this protocol. However, during temperature transitions, spontaneous episodes of VF occurred in 2 of 5 *SCN5A*$^{E558X/+}$ hearts. Sequential activation maps taken shortly after VF initiation demonstrated that activity often began as an organized focal source or broad wavefront on the RV free wall (Figure 5C). Rotors were not observed during any recorded arrhythmia. The organized period of the arrhythmias often lasted several minutes, eventually becoming less organized and showing multiple wave front activity. Triphenyl tetrazolium chloride (TTC) staining was performed to rule out the possibility of frank myocardial ischemia or infarction, which was not seen in *SCN5A*$^{E558X/+}$ or WT hearts (Figure 5D). To explore whether autonomic denervation was responsible for the enhanced arrhythmic phenotype in the mutant hearts, WT (n = 4, age 10 ± 1 months) and *SCN5A*$^{E558X/+}$ (n = 4, age 10 ± 1 months) pigs were treated with a combination of propranolol and atropine to induce autonomic blockade. However, despite chemical denervation, spontaneous ventricular arrhythmias were not observed in *SCN5A*$^{E558X/+}$ pigs (data not shown).

Discussion

SCN5A mutations were first identified in patients with BrS and VF in 1998 (3), yet the mechanism of arrhythmia initiation as well as the arrhythmogenic substrate remain poorly defined. Although the biophysical properties of several disease-causing *SCN5A* mutations have been characterized, integrated understanding of the mechanisms linking sodium channel dysfunction to cardiac pathophysiology is lacking. Here, we developed a genetically engineered porcine model of *SCN5A* haploinsufficiency that recapitulated many features of cardiac sodium channelopathy, including baseline and inducible conduction defects and ventricular arrhythmias. These features showed striking similarities to the human condition and validated the *SCN5A*$^{E558X/+}$ pig as a model system by which to study arrhythmia mechanisms.

The conduction abnormalities observed in *SCN5A*$^{E558X/+}$ pigs functionally phenocopied hereditary PCCD, a syndrome characterized by progressive conduction failure of the HPS leading to bundle branch blocks and AV block. Mutations in *SCN5A* have been identified in families with hereditary PCCD through linkage analysis (1, 22). Similar to PCCD patients and children with loss-of-function *SCN5A* mutations (1, 8), *SCN5A*$^{E558X/+}$ pigs exhibited conduction slowing at an early age that progressively worsened with maturity, as evidenced by an age-dependent sensitivity to flecainide. Lenegre as well as Lev described sclerotic changes in the cardiac conduction system of PCCD patients (23); however, this was not observed in sexually mature *SCN5A*$^{E558X/+}$ pigs, despite ECG evidence of slowed conduction. These results suggest that loss-of-function *SCN5A* mutations associated with PCCD lead to reduced conduction reserve in HPS-derived myocytes that, when coupled with age-related or pathologic fibrosis, can progress to premature conduction failure of the CCS (1).

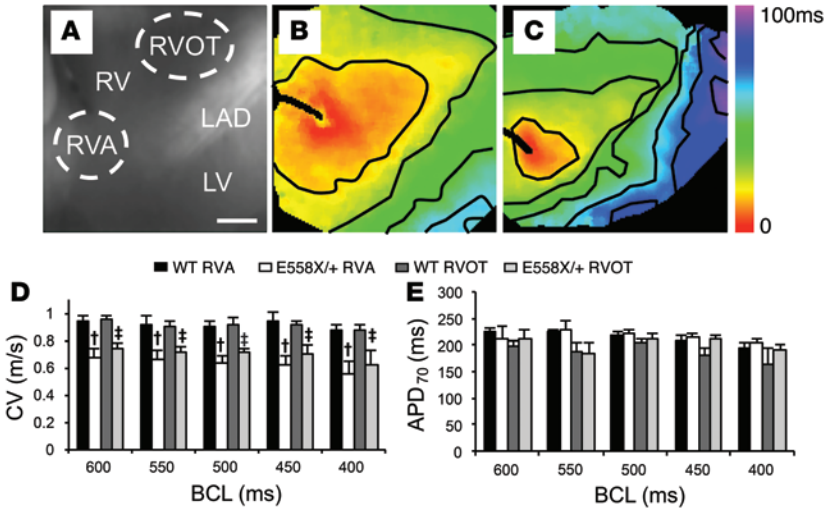

Figure 4. Conduction slowing in the RV free wall of *SCN5A*$^{E558X/+}$ hearts. (**A**) Brightfield image of the RV free wall showing regions where CVs were measured. LAD, left descending artery. Scale bar: 2 cm. (**B** and **C**) Representative activation maps from WT (**B**) and *SCN5A*$^{E558X/+}$ (**C**) hearts. Isochronal lines are drawn every 12.5 ms. (**D** and **E**) Average CV (**D**) and APD (APD_{70}; **E**) measured from the RVA and RVOT of WT and *SCN5A*$^{E558X/+}$ animals. BCL, basic cycle length. $^{\dagger}P < 0.05$ vs. WT RVA; $^{\ddagger}P < 0.05$ vs. WT RVOT.

Interestingly, despite the observation that *SCN5A*$^{E558X/+}$ pigs did not develop a BrS-pattern ECG, even in the presence of high-dose flecainide, isolated *SCN5A*$^{E558X/+}$ hearts were rhythmically unstable, manifesting spontaneous or inducible VF. Although it is simplest to ascribe the absence of the BrS-type ECG to the lack of calcium-independent transient outward K^+ current in the pig heart (24–26), we cannot at this time exclude the role of myocardial fibrosis in the development of ST elevations (27, 28). The phenotype of *SCN5A*$^{E558X/+}$ pigs is comparable to the BrS-negative/PCCD-positive/SCD-positive sodium channelopathy cohorts reported by both Watanabe and Zumhagen (9, 10). Thus, our data suggest that loss of function of sodium channel mutations may be sufficient to sensitize the myocardium to support fibrillatory activity, but multiple factors, whether genetically determined or acquired, must conspire to produce the repolarization heterogeneities or other perturbations responsible for triggering pathologic VPBs and a BrS-pattern ECG (25–31).

Fever is a well-established precipitant of ventricular arrhythmias in loss-of-function *SCN5A* mutant carriers (32–34), including the child we described herein with the E555X mutation. In this regard, it is intriguing that in Langendorff-perfused *SCN5A*$^{E558X/+}$ hearts, we observed increased VF episodes during temperature transitions, but greater stability once steady-state temperatures were reached. It is conceivable that the temperature transitions produce transient electrophysiological heterogeneities that serve to increase the burden of arrhythmic triggers. Thus, temperature fluctuations, rather than fever per se, may explain the proarrhythmic behavior observed in Langendorff-perfused hearts and febrile BrS patients, and conceivably even in BrS patients who develop sudden cardiac death during sleep, when core body temperature may significantly decline (35). It is worth noting that a subset of *SCN5A* mutations displays biophysical abnormalities that may diminish I_{Na} at elevated temperatures, including the sodium window current (36, 37). While we consider it unlikely, it is possible that the truncated protein dominantly influences the biophysical properties of the coexpressed WT α subunit, producing aberrant temperature sensitivity (38). Heterologous expression studies will be required to formally test this possibility.

Spontaneous VF episodes were initiated by isolated or repetitive monomorphic ventricular premature beats. Although initiating VPBs and VF onset were not mapped, due to the stochastic nature of these events, optical mapping after VF initiation demonstrated that arrhythmia activity often began as an organized focal source or broad wavefront in the RV free wall. Interestingly, these data were reminiscent of idiopathic VF originating from the RVOT described by Noda et al.; the authors proposed that rapid firing due to triggered activity or microreentry from the RVOT creates functional block and/or local conduction slowing, giving rise to fibrillatory conduction (39). It is conceivable that this mechanism is contributing to VF in *SCN5A*$^{E558X/+}$ hearts, as reduced I_{Na} would worsen conditions for unidirectional block and set the stage for reentry. In fact, a recent computational simulation suggested that global reductions in I_{Na} could precipitate reentry through source-sink mismatch and conduction block for wavefronts propagating from thin to thick tissue, as would arise in the RVOT (40). Additional studies using simultaneous endocardial/epicardial mapping need to be performed to test this hypothesis.

In summary, the *SCN5A*$^{E558X/+}$ pig model reproduces many of the clinically important features of loss-of-function sodium channelopathies, including conduction disease and increased propensity for ventricular arrhythmias. The *SCN5A*$^{E558X/+}$ pig model represents a significant advance in the study of sodium channel dysfunction and arrhythmogenesis. Arrhythmia mechanisms can now be studied in an organism whose cardiac depolarization and repolarization kinetics are more similar to those of humans, enabling more immediate translation of novel therapeutic modalities to patients at risk for sudden cardiac death.

Methods

Animal studies. The *SCN5A* mutant pigs were generated by homologous recombination in fibroblasts from outbred domestic Yucatan mini pigs. The E558X premature stop mutation was introduced into the *SCN5A* gene, followed by somatic cell nuclear transfer and embryo transfer to generate *SCN5A*$^{E558X/+}$ heterozygous offspring. The targeting vector included the G-to-T point mutation, resulting in replacement of a glutamic acid at amino acid 558 with a premature stop codon (GAG to TAG), a floxed neomycin resistance cassette driven by the phosphoglycerate kinase promoter (Neo^R) in intron 11 for selection, and 5′ and 3′ flanking homology arms (Figure 1B). The targeting vector was introduced into fetal fibroblasts via recombinant adeno-associated virus (rAAV) infection. Successful targeting was confirmed by Southern blot analysis and PCR, using primers flanking the site of integration (Figure 1C). Introduction of the point mutation into the pig genome was confirmed by PCR and direct sequencing (Figure 1D). After nuclear transfer and fusion/

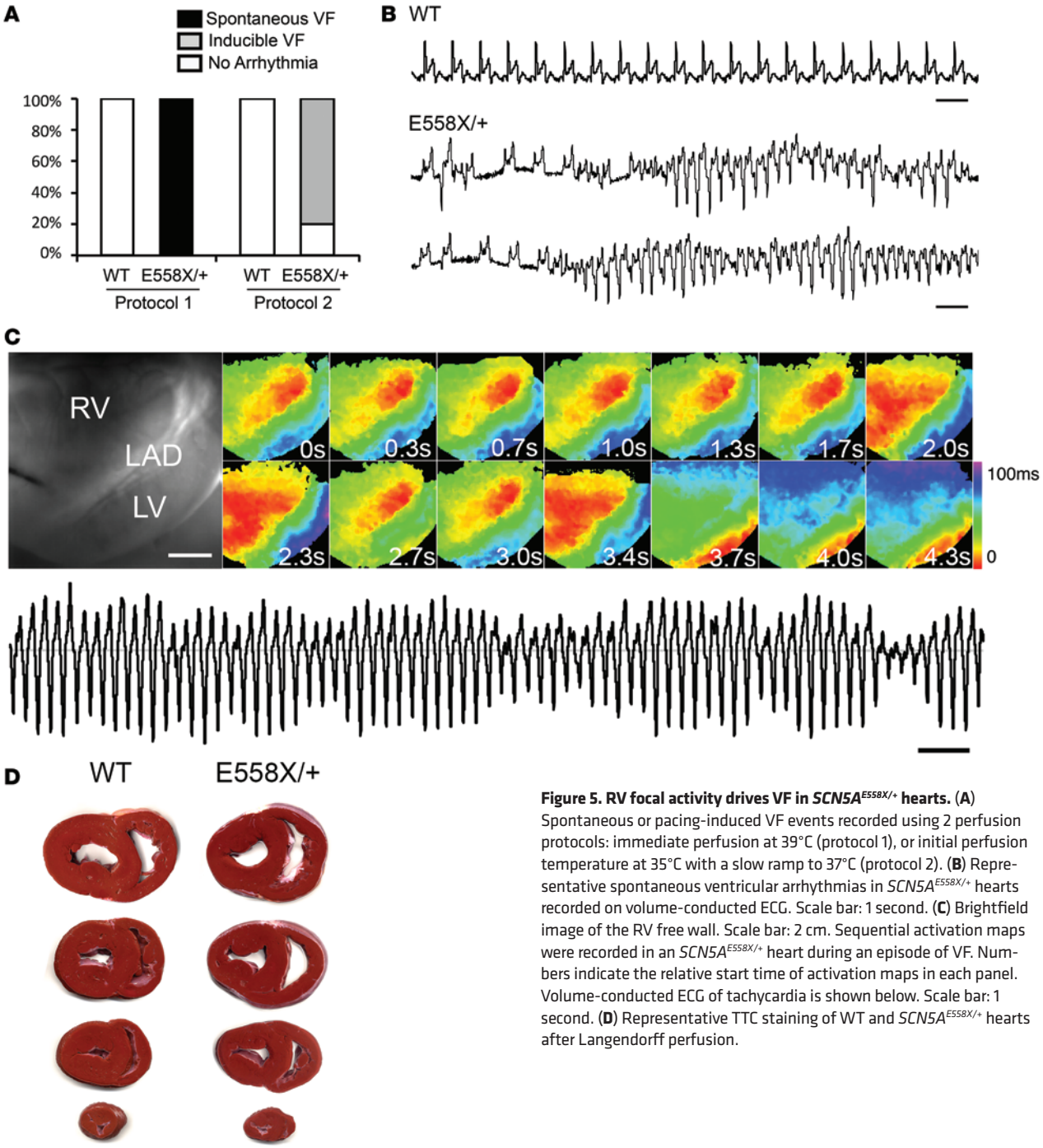

Figure 5. RV focal activity drives VF in *SCN5A*$^{E558X/+}$ hearts. (**A**) Spontaneous or pacing-induced VF events recorded using 2 perfusion protocols: immediate perfusion at 39°C (protocol 1), or initial perfusion temperature at 35°C with a slow ramp to 37°C (protocol 2). (**B**) Representative spontaneous ventricular arrhythmias in *SCN5A*$^{E558X/+}$ hearts recorded on volume-conducted ECG. Scale bar: 1 second. (**C**) Brightfield image of the RV free wall. Scale bar: 2 cm. Sequential activation maps were recorded in an *SCN5A*$^{E558X/+}$ heart during an episode of VF. Numbers indicate the relative start time of activation maps in each panel. Volume-conducted ECG of tachycardia is shown below. Scale bar: 1 second. (**D**) Representative TTC staining of WT and *SCN5A*$^{E558X/+}$ hearts after Langendorff perfusion.

activation, nuclear transfer embryos were transferred to recipient animals. After a 114-day gestation period, the resulting piglets had 1 SCN5A-targeted allele.

Animals were fasted for 18 hours prior to the procedure. Initial sedation was achieved with intramuscular ketamine (33 mg/kg) and atropine (60 μg/kg). An ear vein was catheterized. Sedation was maintained using inhaled isofluorane delivered via nose cone for ECG and drug infusion studies or via direct endotracheal intubation for EPS, electroanatomic mapping, and TTE. Blood pressure and 12-lead ECG were recorded at 5-minute intervals. Adult males were used for all studies except for the baseline ECG analysis and flecainide infusion studies. In the ECG analysis, 5 WT and 5 *SCN5A*$^{E558X/+}$ females were included in each group.

Flecainide infusion protocol. Animals were sedated with intramuscular ketamine (33 mg/kg), and sedation was maintained using inhaled isofluorane delivered via nose cone. Peripheral venous access (ear vein) was then obtained. Flecainide was infused slowly over 10 minutes: each animal received 2 mg/kg flecainide up to a maximum dosage of 150 mg (6, 15), if tolerated. A 12-lead ECG was continuously recorded during infusion, and blood pressure was measured at 2-minute intervals. Infusion was interrupted if advanced conduction block, significant QRS interval widening,

significant hypotension, or sustained ventricular arrhythmias were recorded.

Autonomic blockade protocol. Autonomic blockade was performed as previously described (41). Blood pressure and 12-lead ECG were recorded at 5-minute intervals. Autonomic blockade was administered via ear vein in sedated animals using the following protocol. First, pre-infusion blood pressure and 12-lead ECG was recorded. Second, propranolol hydrochloride (1.0 mg/kg, $t_{1/2}$ = 3–4 hours; Sigma-Aldrich) diluted in 3 ml sterile saline (0.9% sodium chloride) was injected, and blood pressure and 12-lead ECG were recorded at minutes 5, 10, and 15. Third, atropine sulfate (0.1 mg/kg, $t_{1/2}$ = 2 hours; Sigma-Aldrich) was diluted in 3 ml sterile saline and injected at minute 20, and blood pressure and 12-lead ECG were recorded at minutes 25, 30, and 35.

TTE. Imaging was performed with pigs in a partially left lateral recumbent position. A long-axis view was used to measure aortic root diameter and left atrial dimensions. A modified 4-chamber view was used to measure RV inflow diameter. Short-axis views were used to measure RVOT diameter. M-mode ECG taken in short axis was used for quantification of LV wall thickness, LV internal dimensions, and fractional shortening.

EPS. Right and left femoral veins were isolated by blunt surgical dissection. The distal vessels were ligated with a 0-0 silk suture, and the veins were punctured with an 18-gauge angiocatheter. Guide wires were passed under fluoroscopic guidance into the inferior vena cava. 2 sheaths were placed in the right femoral vein, and 1 in the left femoral vein (all sheaths 8 French). A duodecapolar catheter was advanced into the tip of the RVA. 2 hexapolar catheters were advanced and positioned at the high right atrium and at the bundle of His (both catheters 6 French). A comprehensive electrophysiologic study was performed. This included measurement of baseline intervals, atrial pacing with single extrastimuli, atrial incremental pacing, and ventricular pacing with single extrastimuli from the RVA and RVOT. At the end of the experiment, the pigs were euthanized by i.v. injection of beuthanasia (150 mg/kg; Intervet/Schering-Plough Animal Health). Subsequently, hearts were extracted for histological and molecular evaluation or for optical mapping.

Electroanatomic mapping. Detailed mapping of the endocardial and epicardial surface of the RV was performed during sinus rhythm using a 3.5-mm tip Therapy Cool Path Bi-directional Ablation Catheter (St. Jude Medical Inc.), as previously described (27). Pericardial access was performed as previously described (42). Abnormal electrograms were defined as (a) low voltage (≤1.5 mV); (b) fractionated electrograms, with multiple potentials with ≥2 distinct components and >20-ms isoelectric segments between individual components; and (c) long duration (>80 ms) or late potentials, with distinct potentials extending beyond the terminal component of the QRS complex, as modified from a previous report (27).

Antibody reagents. Rabbit anti-Cx43 (Sigma-Aldrich, catalog no. 6219) was used at 1:1,000 for WB and 1:250 for immunofluorescence (IF) staining. Mouse anti–N-cad (BD Biosciences, catalog no. 610921) was used at 1:100 for WB and IF. Rabbit anti–ZO-1 (Invitrogen, catalog no. 61-7300) was used at 1:500 for WB and 1:100 for IF. Rabbit anti-desmoplakin (Serotec, catalog no. 2722-5204) was used at 1:100 for WB and IF. SAP97 monoclonal antibody (Enzo Life Sciences, clone RPI 197.4, catalog no. ADI-VAM-PS005) was used at 1:1,000 for WB and 1:100 for IF. Anti-$Na_v1.5$ was used at 1:500 for WB (Alomone Labs, catalog no. ASC-005) and 1:50 for IF (gift from P. Mohler, Ohio State University Wexner Medical Center, Columbus, Ohio, USA). Anti–ankyrin G mouse monoclonal antibody (Life Technologies, catalog no. 33-8800) was used at 1:200 for WB and 1:100 for IF.

Immunohistochemistry. Hearts were excised and immediately placed in ice-cold PBS. Transmural sections were prepared from the RVOT, LVOT, RVA, and LV apex. Tissue sections were prepared frozen in Tissue Tek OCT compound (Fisher Scientific) or processed for paraffin embedding. For frozen tissues, 8-μm sections were cut and collected on Superfrost/Plus microscope slides (Fisher Scientific) and fixed in 4% paraformaldehyde for 10 minutes before staining. For paraffin sections, 5-μm sections were collected on slides, deparaffinized, and rehydrated, and antigen retrieval step was done with 1× citrate buffer (Biogenex) before proceeding. Sections were blocked with 10% serum and 0.01% Triton in PBS for 1 hour, then incubated with primary antibodies overnight. Sections were then washed in PBS and incubated with secondary antibodies with Alexa Fluor dyes (Invitrogen) for 1 hour before mounting. Slides were coverslipped with Vectashield mounting media with DAPI (Vector Laboratories). Stained sections were visualized on an Axiovert 200M fluorescence microscope. Images were collected using uniform exposure settings for each staining run on an Axiocam camera with AxioVision 4.48 software (Carl Zeiss). Confocal images were taken with a Leica TCS SP5 confocal microscope using Leica LAS AF acquisition software.

Crude ventricular membrane preparation. Membrane lysates were prepared as previously described (20). In brief, 30 mg ventricular tissue from the RVOT or LVOT was excised from frozen tissue blocks. Frozen tissue samples were immediately homogenized in buffer containing 320 mmol/l sucrose, 5 mmol/l EDTA, 5 mmol/l EGTA, 1 mmol/l PMSF, Protease Inhibitor Mixture (Roche), and 20 mmol/l HEPES, pH 7.5. Homogenates were centrifuged at 1,200 *g* for 10 minutes to pellet nuclei. Supernatant was collected and then centrifuged at 100,000 *g* for 1 hour at 4°C. Membrane pellets were resuspended in buffer containing 1% IGEPAL CA-630 (octylphenoxypolyethoxyethanol), 0.1% SDS, 150 mmol/l NaCl, 20 mmol/l HEPES, and Protease Inhibitor Mixture, pH 7.5. The membrane lysate was clarified using ultracentrifugation at 100,000 *g* for 30 minutes at 4°C. Concentrations of membrane lysate preparations were determined using Bradford assay (Bio-Rad).

WB analysis. Samples were run on 4%–20% precast polyacrylamide gradient gels (Invitrogen) and transferred to nitrocellulose (Bio-Rad) overnight at 4°C. Nitrocellulose membranes were incubated in blocking buffer consisting of PBS with Tween-20 (0.05%) and 5% nonfat dry milk. Membranes were then incubated with specific primary antibodies diluted in 5% nonfat dry milk overnight at 4°C followed by wash steps and secondary antibodies (Li-Cor). Antigen complexes were visualized and quantified with the Odyssey Imaging System (Li-Cor).

TTC staining. 1% TTC (Sigma-Aldrich; catalog no. T8877) in saline was prepared immediately prior to use and stored at 37°C. Langendorff-perfused hearts were decannulated and immediately placed in ice-cold Tyrode's solution. Short-axis myocardial sections were covered with 1% TTC solution and incubated in the dark at 37°C for 20 minutes. Stained sections were briefly washed in saline solution prior to imaging.

Dissociated atrial cardiomyocytes. Dissociated atrial cardiomyocytes were prepared from the tips of the left atrial appendage from WT and *SCN5A*$^{E558X/+}$ pigs (43). Whole-cell currents were obtained using standard patch and recording solutions and were generated by step depolarizations from a holding potential of –120 mV.

Optical mapping. Hearts were rapidly excised from WT and *SCN5A*$^{E558X/+}$ animals through a midline thoracotomy. Hearts were transported to the mapping laboratory in cold (0°C) Tyrode's solution. The aortas were cannulated, and hearts were Langendorff perfused with Tyrode's solution at 39°C (protocol 1) or at 35°C with slow ramp to 37°C (protocol 2). High-resolution optical mapping of the epicardial surface was performed as previously described (44). In brief, hearts were initially perfused with Tyrode's solution to clear the blood and stabilize the heart, followed by Tyrode's solution containing 10 μM blebbistatin. The voltage-sensitive dye Di-4-ANNEPS (Molecular Probes Inc.) was then perfused as a 1-mg bolus. Light from green LEDs (530 nm; Luxeon LED Inc.) was used as an excitation source, and the emitted light (>590 nm) was detected with 2 high-resolution CCD cameras (Dalsa Inc., catalog no. CA-D1 128) with 128 × 128 pixel resolution at 400 frames per second. Images were digitized and analyzed using a custom software package.

Statistics. Quantitative values are expressed as mean ± SD. 2-tailed Student's *t* test was used to compare differences in continuous variables between *SCN5A*$^{E558X/+}$ and control animals. 2-way ANOVA was used to assess the interaction between age and genotype on continuous ECG variables. CV and APD values were compared using 2-way ANOVA. A *P* value less than 0.05 was considered statistically significant. The SPSS statistical package (version 20.0; IBM) was used for analyses.

Study approval. This study was carried out in accordance with the recommendations in the NIH *Guide for the Care and Use of Laboratory Animals*. All animals were developed and housed in the AAALAC-accredited facilities of Exemplar Genetics. Standard procedures for animal husbandry were used throughout. The IACUC of Exemplar Genetics and New York University School of Medicine approved all animal experiments.

Acknowledgments

The authors thank Cindy Loomis and Mark Alu of the Histopathology Core (supported in part by grant 5P30CA016087-32 from the National Cancer Institute), as well as Yu Guo for assistance with statistical analysis.

Address correspondence to: Glenn I. Fishman, Leon H. Charney Division of Cardiology, New York University School of Medicine, 522 First Avenue, Smilow 801, New York, New York 10016, USA. Phone: 212.263.3967; E-mail: glenn.fishman@nyumc.org.

1. Probst V, et al. Haploinsufficiency in combination with aging causes SCN5A-linked hereditary Lenegre disease. *J Am Coll Cardiol*. 2003;41(4):643–652.
2. Kyndt F, et al. Novel SCN5A mutation leading either to isolated cardiac conduction defect or Brugada syndrome in a large French family. *Circulation*. 2001;104(25):3081–3086.
3. Chen Q, et al. Genetic basis and molecular mechanism for idiopathic ventricular fibrillation. *Nature*. 1998;392(6673):293–296.
4. Amin AS, et al. Facilitatory and inhibitory effects of SCN5A mutations on atrial fibrillation in Brugada syndrome. *Europace*. 2011;13(7):968–975.
5. McNair WP, et al. SCN5A mutations associate with arrhythmic dilated cardiomyopathy and commonly localize to the voltage-sensing mechanism. *J Am Coll Cardiol*. 2011;57(21):2160–2168.
6. Antzelevitch C, et al. Brugada syndrome: report of the second consensus conference: endorsed by the Heart Rhythm Society and the European Heart Rhythm Association. *Circulation*. 2005;111(5):659–670.
7. Ackerman MJ, et al. HRS/EHRA expert consensus statement on the state of genetic testing for the channelopathies and cardiomyopathies: this document was developed as a partnership between the Heart Rhythm Society (HRS) and the European Heart Rhythm Association (EHRA). *Europace*. 2011;13(8):1077–1109.
8. Chockalingam P, et al. The diagnostic and therapeutic aspects of loss-of-function cardiac sodium channelopathies in children. *Heart Rhythm*. 2012;9(12):1986–1992.
9. Watanabe H, et al. Electrocardiographic characteristics and SCN5A mutations in idiopathic ventricular fibrillation associated with early repolarization. *Circ Arrhythm Electrophysiol*. 2011;4(6):874–881.
10. Zumhagen S, et al. A heterozygous deletion mutation in the cardiac sodium channel gene SCN5A with loss- and gain-of-function characteristics manifests as isolated conduction disease, without signs of Brugada or long QT syndrome. *PLoS One*. 2013;8(6):e67963.
11. Rogers CS, et al. Production of CFTR-null and CFTR-DeltaF508 heterozygous pigs by adeno-associated virus-mediated gene targeting and somatic cell nuclear transfer. *J Clin Invest*. 2008;118(4):1571–1577.
12. Stubhan M, et al. Evaluation of cardiovascular and ECG parameters in the normal, freely moving Gottingen Minipig. *J Pharmacol Toxicol Methods*. 2008;57(3):202–211.
13. Maury P, et al. Prevalence and prognostic role of various conduction disturbances in patients with the brugada syndrome. *Am J Cardiol*. 2013;112(9):1384–1389.
14. Probst V, et al. Progressive cardiac conduction defect is the prevailing phenotype in carriers of a Brugada syndrome SCN5A mutation. *J Cardiovasc Electrophysiol*. 2006;17(3):270–275.
15. Brugada R, et al. Sodium channel blockers identify risk for sudden death in patients with ST-segment elevation and right bundle branch block but structurally normal hearts. *Circulation*. 2000;101(5):510–515.
16. Cerrone M, Delmar M. Desmosomes and the sodium channel complex: implications for arrhythmogenic cardiomyopathy and Brugada syndrome. *Trends Cardiovasc Med*. 2014;24(5):184–190.
17. Delmar M. Connexin43 regulates sodium current; ankyrin-G modulates gap junctions: the intercalated disc exchanger. *Cardiovasc Res*. 2012;93(2):220–222.
18. Jansen JA, et al. Reduced heterogeneous expression of Cx43 results in decreased Nav1.5 expression and reduced sodium current which accounts for arrhythmia vulnerability in conditional Cx43 knockout mice. *Heart Rhythm*. 2012;9(4):600–607.
19. Sato PY, et al. Loss of plakophilin-2 expression leads to decreased sodium current and slower conduction velocity in cultured cardiac myocytes. *Circ Res*. 2009;105(6):523–526.
20. Milstein ML, et al. Dynamic reciprocity of sodium and potassium channel expression in a macromolecular complex controls cardiac excitability and arrhythmia. *Proc Natl Acad Sci U S A*. 2012;109(31):E2134–E2143.
21. Wilde AA, et al. The pathophysiological mechanism underlying Brugada syndrome: depolarization versus repolarization. *J Mol Cell Cardiol*. 2010;49(4):543–553.
22. Schott JJ, et al. Cardiac conduction defects associate with mutations in SCN5A. *Nat Genet*. 1999;23(1):20–21.
23. Lev M. Anatomic basis for atrioventricular block. *Am J Med*. 1964;37(5):742–748.
24. Li GR, Du XL, Siow YL, O K, Tse HF, Lau CP. Calcium-activated transient outward chloride current and phase 1 repolarization of swine ventricular action potential. *Cardiovasc Res*. 2003;58(1):89–98.
25. Yan GX, Antzelevitch C. Cellular basis for the electrocardiographic J wave. *Circulation*. 1996;93(2):372–379.
26. Yan GX, Antzelevitch C. Cellular basis for the Brugada syndrome and other mechanisms of arrhythmogenesis associated with ST-segment elevation. *Circulation*. 1999;100(15):1660–1666.
27. Nademanee K, et al. Prevention of ventricular fibrillation episodes in Brugada syndrome by catheter ablation over the anterior right ventricular outflow tract epicardium. *Circulation*. 2011;123(12):1270–1279.
28. Frustaci A, et al. Cardiac histological substrate in patients with clinical phenotype of Brugada syndrome. *Circulation*. 2005;112(24):3680–3687.
29. Bezzina CR, et al. Common variants at SCN5A-SCN10A and HEY2 are associated with Brugada syndrome, a rare disease with high risk of sudden

cardiac death. *Nat Genet*. 2013;45(9):1044–1049.
30. Gang ES, Priori SS, Chen PS. Short coupled premature ventricular contraction initiating ventricular fibrillation in a patient with Brugada syndrome. *J Cardiovasc Electrophysiol*. 2004;15(7):837.
31. Kakishita M, et al. Mode of onset of ventricular fibrillation in patients with Brugada syndrome detected by implantable cardioverter defibrillator therapy. *J Am Coll Cardiol*. 2000;36(5):1646–1653.
32. Amin AS, Meregalli PG, Bardai A, Wilde AA, Tan HL. Fever increases the risk for cardiac arrest in the Brugada syndrome. *Ann Int Med*. 2008;149(3):216–218.
33. Antzelevitch C, Brugada R. Fever and Brugada syndrome. *Pacing Clin Electrophysiol*. 2002;25(11):1537–1539.
34. Keller DI, et al. Brugada syndrome and fever: genetic and molecular characterization of patients carrying SCN5A mutations. *Cardiovasc Res*. 2005;67(3):510–519.
35. Krauchi K, Wirz-Justice A. Circadian rhythm of heat production, heart rate, and skin and core temperature under unmasking conditions in men. *Am J Physiol*. 1994;267(3 Pt 2):R819–R829.
36. Dumaine R, et al. Ionic mechanisms responsible for the electrocardiographic phenotype of the Brugada syndrome are temperature dependent. *Circ Res*. 1999;85(9):803–809.
37. Mok NS, Priori SG, Napolitano C, Chan NY, Chahine M, Baroudi G. A newly characterized SCN5A mutation underlying Brugada syndrome unmasked by hyperthermia. *J Cardiovasc Electrophysiol*. 2003;14(4):407–411.
38. Clatot J, et al. Dominant-negative effect of SCN5A N-terminal mutations through the interaction of Na(v)1.5 alpha-subunits. *Cardiovasc Res*. 2012;96(1):53–63.
39. Noda T, et al. Malignant entity of idiopathic ventricular fibrillation and polymorphic ventricular tachycardia initiated by premature extrasystoles originating from the right ventricular outflow tract. *J Am Coll Cardiol*. 2005;46(7):1288–1294.
40. Boyle PM, Park CJ, Arevalo HJ, Vigmond EJ, Trayanova NA. Sodium current reduction unmasks a structure-dependent substrate for arrhythmogenesis in the normal ventricles. *PLoS One*. 2014;9(1):e86947.
41. Poletto R, et al. Identification of low and high frequency ranges for heart rate variability and blood pressure variability analyses using pharmacological autonomic blockade with atropine and propranolol in swine. *Physiol Behav*. 2011;103(2):188–196.
42. Sosa E, Scanavacca M, d'Avila A, Pilleggi F. A new technique to perform epicardial mapping in the electrophysiology laboratory. *J Cardiovasc Electrophysiol*. 1996;7(6):531–536.
43. Bustamante JO, Watanabe T, Murphy DA, McDonald TF. Isolation of single atrial and ventricular cells from the human heart. *Can Med Assoc J*. 1982;126(7):791–793.
44. Pandit SV, et al. Targeting atrioventricular differences in ion channel properties for terminating acute atrial fibrillation in pigs. *Cardiovasc Res*. 2011;89(4):843–851.